Site-Specific Recoil Diffraction of Backscattered Electrons in Crystals

Aimo Winkelmann
Max-Planck-Institut für Mikrostrukturphysik, Weinberg 2, D-06120 Halle(Saale), Germany

Maarten Vos
Research School of Physics and Engineering, Australian National University, Canberra ACT, Australia
(Received 12 November 2010; published 24 February 2011)

A novel diffraction effect in high-energy electron backscattering is demonstrated: the formation of element-specific diffraction patterns via nuclear recoil. For sapphire (Al_2O_3), the difference in recoil energy allows us to determine if an electron scattered from aluminum or from oxygen. The angular electron distribution obtained in such measurements is a strong function of the recoiling lattice site. These element-specific recoil diffraction features are explained using the dynamical theory of electron diffraction. Our observations open up new possibilities for local, element-resolved crystallographic analysis using quasielastically backscattered electrons in scanning electron microscopy.

DOI: 10.1103/PhysRevLett.106.085503 PACS numbers: 61.05.J−, 68.37.Hk, 68.49.Jk

An electron beam with energy E_0 can be elastically and coherently scattered when it is either transmitted through a thin crystal or reflected at its surface. Diffracted electron beams at E_0 are then geometrically allowed only in directions which correspond to wave vector changes by a reciprocal lattice vector [1]. In such a coherent process, the recoil momentum is taken up collectively by the crystal and negligible recoil energy E_R is transferred from the diffracted electrons to the crystal.

Recoil energy can also be transferred between the incident electron and phonon excitations. In transmission high-energy electron diffraction, the forward scattering geometry implies a small momentum transfer $\boldsymbol{K}$ and the resulting recoil energy is below the current energy resolution limits. In contrast, when using large scattering angles in a reflection geometry, the recoil energy transferred by the electron can easily reach a few eV for $E_0 > 10$ keV. In this case, the recoil energy is well above the single phonon response spectrum, and the transfer of momentum is to a single atom, rather than to the crystal as a whole, while the scattering is incoherent [2]. The recoil event distinguishes atoms of different masses M_A via their contribution at an energy loss of $E_R(A) = K^2/2M_A$ in electron Rutherford backscattering spectroscopy (ERBS) [3–7]. Similarly, electron-induced recoil effects can also play a role in x-ray photoelectron and Auger spectroscopy [8–11].

The problem of localized versus delocalized transfer of recoil energy and momentum is of very general importance for the diffraction physics of electrons, neutrons and x rays in crystals. The application of ERBS in reflection high-energy electron diffraction measurements allows us for the first time to directly investigate the implications of *localized* nuclear recoil for the formation of different types of electron diffraction patterns. Moreover, the experimental access to *element-specific* recoil-resolved backscattered electron diffraction patterns would open up new possibilities for crystallographic analyses, e.g., in the scanning electron microscope (SEM). Here, we demonstrate element-specific localization of high-energy electron backscattering in a sapphire (Al_2O_3) crystal. We use the recoil energy loss to identify two inequivalent lattice sites where incoherent scattering occurs. By comparing the measured diffraction features with dynamical electron diffraction simulations, they are identified as Kikuchi patterns [1,12] due to Bragg scattering of electrons from point sources inside a crystal.

The experiments were carried out using an electrostatic high-energy electron loss spectrometer described elsewhere [13,14]. Electrons were detected at a constant scattering angle of 135.7° and $E_0 = 40$ keV incident beam energy (current ≈ 5 nA) with an energy resolution ΔE of ≈ 0.5 eV. The setup (Fig. 1) allows angle-resolved detection of electrons on part of a cone of constant scattering angle. The angular sensitivity is provided by a position sensitive detector consisting of channel plates and a resistive anode. This detector is calibrated for energy and ϕ as described in [13]. The device-grade sapphire $Al_2O_3(0001)$ wafer was measured without further treatment. All measurements were taken at room temperature under ultrahigh vacuum conditions ($p < 5 \times 10^{-10}$ mbar). The detection efficiency of the analyzer as a function of ϕ was determined by measuring the intensity distribution of electrons scattered from a polycrystalline metal shim, where no angular variations are expected. In this way the sapphire angular distributions were corrected for variations in angular detection efficiency.

As an example, we show in Fig. 2 the spectra for electrons scattered into a ϕ range ($3° < \phi < 4°$) for two sample orientations differing in ϑ by only 1° [15]. A small amount (well below a monolayer) of gold was deposited on the sapphire sample. The recoil losses for Au, Al, and O are clearly resolved, as the spectrum shows three peaks.

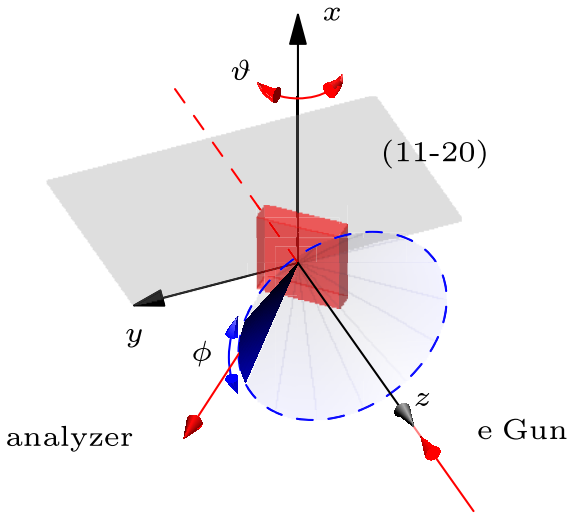

FIG. 1 (color online). Scattering geometry. Energy-resolved detection along a cone of constant scattering angle (135.7°) over a region of $\Delta\phi \approx \pm 5°$. Specific sample orientations for the diffraction profile measurements (Fig. 3) are selected by the angle θ, with the sapphire (11–20) lattice plane approximately in the yz plane.

Moreover, we see a strong influence of the sample orientation on the relative Al and O peak heights. The approximately constant Au peak is consistent with the expected absence of backscattering diffraction effects for statistically distributed atoms on a surface. The observed peak separation is slightly smaller than the expected recoil separation for $E_0 = 40$ keV as is shown in Fig. 2. This difference between the observed and calculated separation indicates that the insulating Al_2O_3 sample charged by ≈ 5 keV due to the impinging electron beam [15].

The initial measurements, shown in Fig. 2, already indicate a strong influence of diffraction on the angular distribution of electrons scattered from the different elements. To analyze this in detail, we used a clean sapphire sample with the (11–20) lattice plane oriented in the yz measurement plane (see Fig. 1). The measured spectra were fitted by two Gaussian peaks centered at the energy loss values corresponding to the Al and O recoil energies, respectively. In Fig. 3 we show the element-resolved peak intensities as a function of the exit angle ϕ and compare them to simulations. The panels show data for three constant incidence angles, with the $\phi = 0°$ exit direction corresponding, respectively, to the [0001] surface normal (top), 4° (middle), and 10° (bottom) away from [0001] in the (11–20) plane. The Al peak has generally higher intensity than the O peak, as expected from the roughly

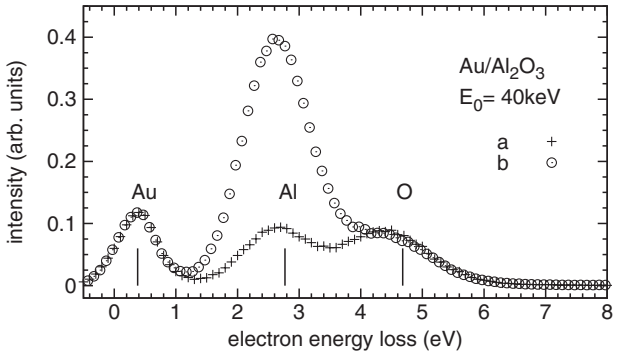

FIG. 2. Angle-resolved energy loss spectra of quasielastically scattered electrons from sapphire (Al_2O_3) with Au atoms deposited on the surface. Data (a) and (b) were measured for two different sample orientations, with ϑ changed by 1°, and integrated for $3° < \phi < 4°$ (see Fig. 1). The vertical lines indicate the mean recoil energy loss values for Au, Al, and O at $E_0 = 40$ keV.

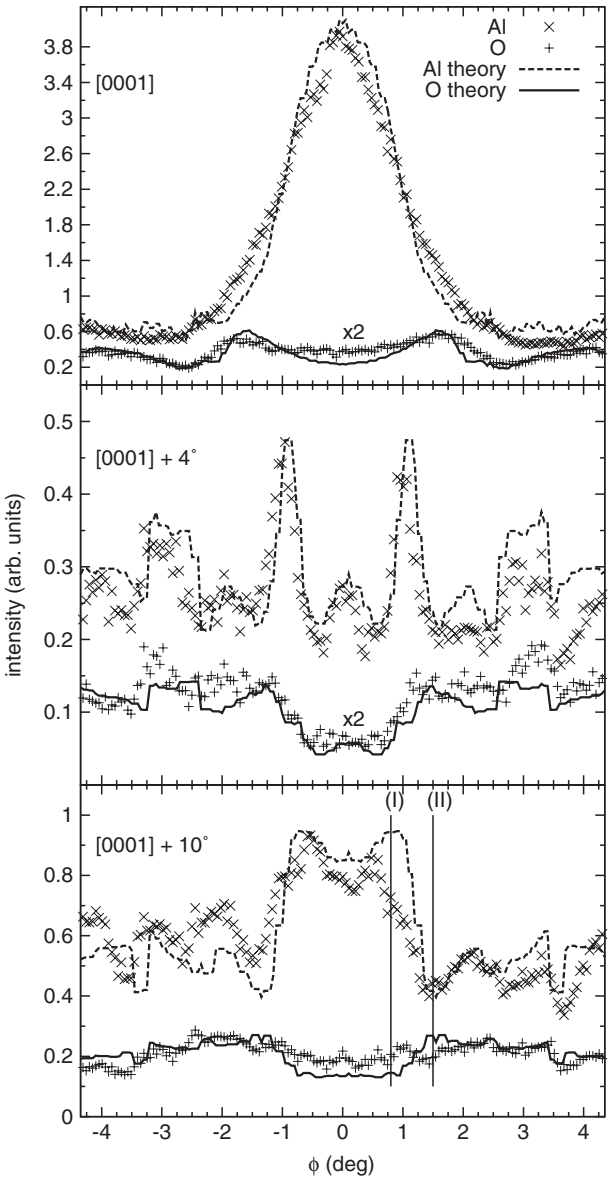

FIG. 3. Comparison of measured intensities (symbols) and simulated ones (lines) of the Al and O quasielastic peaks for three different cuts through the (11–20) Kikuchi band of sapphire. The directions used in panels (I) and (II) of Fig. 4 are indicated in the plot of the [0001] + 10° case.

Z^2-proportional cross section. However, the ϕ dependence of the element-resolved intensities is dramatically different. The top panel of Fig. 3 shows that Al has a strong intensity maximum at $\phi = 0°$, while O has a slight minimum along this [0001] direction. Similarly, in the bottom panel 10° away from [0001], Al shows a band of increased intensity from $-1° < \phi < 1°$, while O shows here a band of decreased intensity. These very different profiles all present cross sections of the (11–20) Kikuchi band. This demonstrates clearly that the shape of the Kikuchi bands is element specific.

These intriguing observations are compared to dynamical electron diffraction simulations which are shown in Fig. 3 as solid (O) and dotted lines (Al). In these simulations, we calculated the dynamical diffraction along the exit pathway after incoherent emission of backscattered electrons from the Al or the O sites, respectively. Based on time-reversal symmetry, the probability of escaping from the Al and O sites into the outgoing direction $+\vec{\mathbf{k}}$ is the same as the overlap of the wave field of a dynamically scattered ingoing plane wave along $-\vec{\mathbf{k}}$ with the atomic backscattering sources [16–18].

The dynamical diffraction calculations were carried out for trigonal Al_2O_3 (space group $R\bar{3}c$) with $a = 4.76$ Å and $c = 12.99$ Å [19]. About 1500 reflecting planes with $d_{hkl} > 0.35$ Å were taken into account. A mean square displacement of 0.01 Å^2 (both for Al and O) was used to calculate the Debye-Waller factor. An inelastic mean free path of 200 Å was used. Charging effects of the sample were treated by assuming an incident energy of 35 keV. The effect of incident beam diffraction is constant for a selected sample orientation and is treated by a scaling factor changing the ratio of the Al and O signal. The ratio of the maximum and minimum intensity for each element (as a function of ϕ) is not affected by this scaling factor and can thus be compared to the experimentally obtained ones. The conclusions presented here are quite general and do not depend sensitively on any of the chosen parameters.

While the dynamical simulation in Fig. 3 shows overall good agreement with the experimental data, the physical mechanism behind the element-specific electron diffraction profiles is more clearly revealed by a simplified calculation using only the 12 strongest reflecting lattice planes perpendicular to the surface. In the middle row of Fig. 4 we show the backscattered intensity from Al (left) and O (right) in an extended two-dimensional angular region near the central [0001] zone axis. Most notably, the horizontal (11–20) Kikuchi band shows a maximum for Al and a minimum for O away from the central [0001] region, as has been measured in the middle and lower panels of Fig. 3. However, there are also other bands (such as the vertical (10–10) Kikuchi band) which show very similar intensity distribution for both elements, with high intensity in the middle of the band.

Panels (I)–(IV) in Fig. 4 show real-space intensity distributions inside the sapphire crystal formed by diffracted

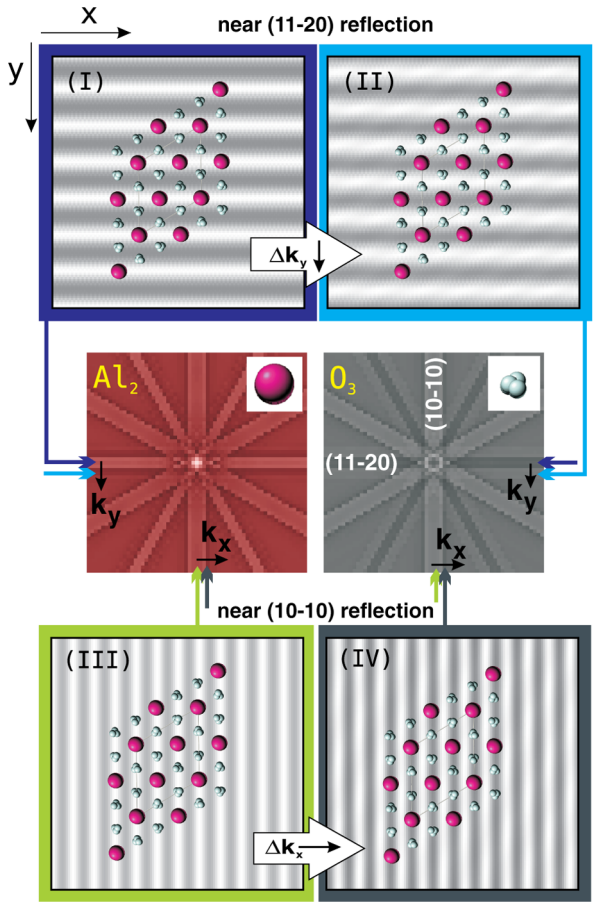

FIG. 4 (color online). Real-space mechanism of site-specific Kikuchi pattern formation in sapphire (Al_2O_3). Panels (I)–(IV) show the real-space probability distribution for scattering into the $\vec{\mathbf{k}}$ directions indicated in the middle panels. The overlap of this distribution with the atomic positions determines the respective element-resolved intensities (see text).

plane waves incident from different $-\vec{\mathbf{k}}$ directions. The intensity is projected along the surface normal direction and is equivalent to the x, y-dependent *exit* probability density for the direction $+\vec{\mathbf{k}}$. The two pairs of $\vec{\mathbf{k}}$ points are near the Bragg angle of two different lattice planes, as indicated by the pairs of arrows near the respective Kikuchi band edges. Panels (I) and (II) straddle the (11–20) Bragg angle, and the corresponding exit angles are also indicated in Fig. 3 in the lower panel. Moving over the horizontal (11–20) Bragg reflection from just inside (I) to just outside (II) the band edge, the exit probability density changes from strong overlap with the Al atomic sites to small overlap with Al, corresponding to high and low intensity of the Al recoil peak in the two different directions, respectively. This process is inverted for the O sites: inside the (11–20) band, the exit probability density is low at O [dark regions in (I)], while outside it becomes high at O [light regions in (II)]. In this way, different (11–20) profiles are produced for O and Al due to their arrangement in separate physical planes for the (11–20) Bragg reflection. The situation is different for the vertical (10–10) band, as

we see in panels (III) and (IV). Here the Al and O atoms are in the same physical planes. Moving over a Bragg reflection from (III) to (IV), the overlap of the exit probability density with the Al and O atoms changes in the same way, producing for both the O and Al sites high intensity inside the band and low intensity outside.

We note that, by reciprocity, the *incident* beam diffraction effects modify the excitation ratios of Al and O sites in a similar way as shown in Fig. 4. This means that the ratio of the primary beam excitation of O to Al sites is not constant ($3Z_O^2/2Z_{Al}^2 = 0.56$, assuming Rutherford cross sections), but depends on the incidence angle. Away from major zone axes, we estimate these variations to be of the order of a factor 2 (as seen in Fig. 3), which is also consistent with the factors used to scale the simulations for different incidence angles in Fig. 3. These incident beam effects will be investigated in the future.

The results presented here immediately suggest applications for SEM-based crystallography, like electron channeling patterns [20] or electron backscatter diffraction [21,22] with energy resolution [23]. With resolution of the recoil losses, element-specific crystallographic information is obtained in a similar way as in channeling-enhanced microanalysis in the TEM [24]. This will greatly enhance the potential of SEM methods for phase identification in materials science. For instance, as hydrogen atoms are well resolved in ERBS [25], our results suggest a new electron-spectroscopic method, sensitive to the position of hydrogen in crystals [26].

From a more fundamental point of view, our results shed light on the processes by which, with increasing recoil energy, quasielastically backscattered electron waves are effectively decoupled from the incident beam with respect to their phase. While the incident and the outgoing pathways are still largely governed by coherent forward scattering, we have shown here that an experimentally identifiable source of dephasing is introduced by nuclear recoil. Our observations thus resolve a long-standing question concerning the physical mechanism that causes the quasielastic incoherent contribution in backscattered Kikuchi electron diffraction patterns [12,27].

In the phonon picture, the recoil induced by the backscattered electron creates a multiphonon wave packet. It is known from neutron scattering theory that, in the limit of large momentum transfer, such multiphonon excitation corresponds to the quasifree recoil of an oscillating atom in the crystal [28]. After the backscattered electron has left the atomic recoil site, the localized excitation spreads over the lattice with time. In this way, the recoil energy is delocalized and thermalized by the phonon subsystem. With the advent of ultrafast electron diffraction techniques [29], time-resolved analysis of this process might become possible.

In conclusion, we have demonstrated and analyzed the formation of site-specific Kikuchi diffraction patterns via element-resolved nuclear recoil of atoms at crystallographically inequivalent sites in sapphire. Our observations provide the basis for improved local phase identification in SEM-based crystallographic methods.

This work was made possible by financial support of the Australian Research Council.

[1] J. M. Cowley, *Diffraction Physics* (North-Holland, Amsterdam, 1995), 3rd ed.
[2] G. I. Watson, J. Phys. Condens. Matter **8**, 5955 (1996).
[3] H. Boersch, R. Wolter, and H. Schoenebeck, Z. Phys. **199**, 124 (1967).
[4] D. Laser and M. P. Seah, Phys. Rev. B **47**, 9836 (1993).
[5] G. Gergely *et al.*, Vacuum **61**, 107 (2001).
[6] M. Vos, Phys. Rev. A **65**, 12 703 (2001).
[7] M. R. Went and M. Vos, Nucl. Instrum. Methods Phys. Res., Sect. B **266**, 998 (2008).
[8] Y. Takata *et al.*, Phys. Rev. Lett. **101**, 137601 (2008).
[9] M. Vos, M. R. Went, Y. Kayanuma, S. Tanaka, Y. Takata, and J. Mayers, Phys. Rev. B **78**, 024301 (2008).
[10] K. Kreidi *et al.*, Phys. Rev. Lett. **103**, 033001 (2009).
[11] S. Suga *et al.*, New J. Phys. **11**, 073025 (2009).
[12] S. A. Chambers, Surf. Sci. Rep. **16**, 261 (1992).
[13] M. Vos, G. P. Cornish, and E. Weigold, Rev. Sci. Instrum. **71**, 3831 (2000).
[14] A. Winkelmann, K. Aizel, and M. Vos, New J. Phys. **12**, 053001 (2010).
[15] M. Vos, K. Aizel, and A. Winkelmann, Surf. Sci. **604**, 893 (2010).
[16] C. J. Rossouw, P. R. Miller, T. W. Josefsson, and L. J. Allen, Philos. Mag. A **70**, 985 (1994).
[17] A. Winkelmann, C. Trager-Cowan, F. Sweeney, A. P. Day, and P. Parbrook, Ultramicroscopy **107**, 414 (2007).
[18] A. Winkelmann, C. S. Fadley, and F. J. Garcia de Abajo, New J. Phys. **10**, 113002 (2008).
[19] S. Pillet, M. Souhassou, C. Lecomte, K. Schwarz, P. Blaha, M. Rérat, A. Lichanot, and P. Roversi, Acta Crystallogr. Sect. A **57**, 290 (2001).
[20] D. C. Joy, D. E. Newbury, and D. L. Davidson, J. Appl. Phys. **53**, R81 (1982).
[21] J. A. Venables and C. J. Harland, Philos. Mag. **27**, 1193 (1973).
[22] *Electron Backscatter Diffraction in Materials Science*, edited by A. J. Schwartz, M. Kumar, B. L. Adams, and D. P. Field (Springer, Berlin, 2009), 2nd ed.
[23] A. Deal, T. Hooghan, and A. Eades, Ultramicroscopy **108**, 116 (2008).
[24] J. Taftø and Z. Liliental, J. Appl. Crystallogr. **15**, 260 (1982).
[25] M. Vos, Ultramicroscopy **92**, 143 (2002).
[26] S. D. Findlay *et al.*, Appl. Phys. Express **3**, 116603 (2010).
[27] O. C. Wells, Scanning **21**, 368 (1999).
[28] J. M. F. Gunn and M. Warner, Z. Phys. B **56**, 13 (1984).
[29] P. Baum and A. H. Zewail, Chem. Phys. **366**, 2 (2009).